Electronic Supplementary Material (ESI) for Physical Chemistry Chemical Physics.
This journal is © the Owner Societies 2015

Supporting Information for

A new approach to elucidating repair reactions of resveratrol

*C. Kerzig, S. Henkel and M. Goez**

Contents

1 The hydrated electron $\mathbf{e}_{\mathbf{aq}}^{\bullet-}$: observation, blanking, and signal separation

As previously,[S1] we recorded the spectrum of $\mathbf{e}_{\mathbf{aq}}^{\bullet-}$ direct in our reaction medium through 266 nm photoionization of water and calibrated it by using the published maximum value ($\varepsilon_{\mathrm{max}} = 22700\,\mathrm{M^{-1}cm^{-1}}$)[S2]. It would seem natural to monitor $\mathbf{e}_{\mathbf{aq}}^{\bullet-}$ at the wavelength of its absorption maximum, 717 nm in our case. However, the emission spectrum of our light source (a high pressure xenon lamp) characteristically exhibits a strong, narrow peak at 824 nm, which results in a much higher photon flux than at 717 nm. Coupled with the fact that the molar absorption coefficient of $\mathbf{e}_{\mathbf{aq}}^{\bullet-}$ is still three quarters of the maximum value ($\varepsilon_{824} = 16900\,\mathrm{M^{-1}\,cm^{-1}}$), observing $\mathbf{e}_{\mathbf{aq}}^{\bullet-}$ at the longer wavelength thus greatly improves the sensitivity. As an additional benefit, the by-product of $\mathbf{e}_{\mathbf{aq}}^{\bullet-}$ in our system, the radical $\mathbf{ResO}^{\bullet}$, also absorbs significantly at 717 nm but is almost transparent at 824 nm (compare, Figure 1a of the main paper).

A convenient means of blanking $\mathbf{e}_{\mathbf{aq}}^{\bullet-}$ is provided by N_2O, which scavenges $\mathbf{e}_{\mathbf{aq}}^{\bullet-}$ selectively and rapidly according to Equation S1,[S3]

$$\mathbf{e}_{\mathbf{aq}}^{\bullet-} + N_2O + H_2O \longrightarrow N_2 + HO^{\bullet} + HO^{-} \qquad \text{(S1)}$$

When the solution is saturated with N_2O, that reaction is completed within the duration of our laser pulses, so practically instantaneously and quantitatively converts the strongly absorbing $\mathbf{e}_{\mathbf{aq}}^{\bullet-}$ into nonabsorbing hydroxyl radicals. As Figure S1 (bottom) illustrates, the remaining small

contribution of **ResO•**, which amounts to less than 5 % of the signal in Ar-saturated solution immediately after the laser pulse, can be reliably detected by that method. Analogously, the pure $\mathbf{e}_{\mathbf{aq}}^{\bullet-}$ signal can be extracted by taking the difference of the traces recorded in Ar-saturated and N_2O-saturated solution with all other experimental parameters unmodified (see, Figure S1, top).

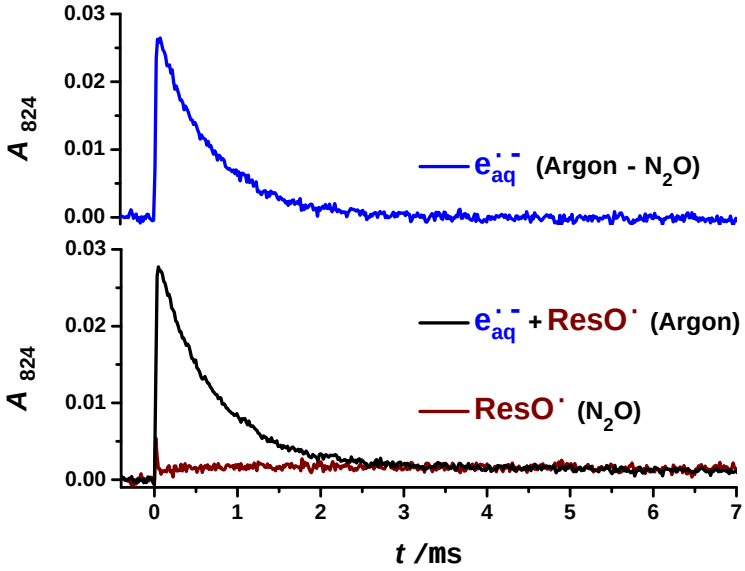

Figure S1: Separation of the **ResO•** and $\mathbf{e}_{\mathbf{aq}}^{\bullet-}$ absorptions in 355 nm laser flash photolysis (349 mJ cm^{-2}) on an aqueous solution of 8×10^{-5} M **ResOH** at pH 6.5. Bottom, experimental absorption traces at 824 nm in Ar-saturated solution (black, both species contributing) and in N_2O-saturated solution (dark red, only **ResO•** contributing). Top, difference of the two traces yielding the pure $\mathbf{e}_{\mathbf{aq}}^{\bullet-}$ signal.

The reaction with N_2O turns the strongly reducing species $\mathbf{e}_{\mathbf{aq}}^{\bullet-}$ into the strongly oxidizing hydroxyl radical, which is in turn scavenged by **ResOH** or any of our co-antioxidants with a rate constant at or near the diffusion-controlled limit.[S4–S6] In the samples containing only **ResOH** that process is not very fast because we employed that reactant in concentrations below 10^{-4} M; the scavenging accounts for the slow secondary growth of **ResO•** (formed via a hydroxyl adduct of **ResOH** that subsequently eliminates water)[S6] in N_2O-saturated solutions that can be perceived in Figures S1 or S5, but does not interfere with the concentration determination immediately after the laser pulse. In contrast, in our investigations of the **ResO•** repair, we applied the regenerating co-antioxidants in 12.5-fold to 1250-fold excess over **ResOH**, so the scavenging of the hydroxyl radicals is almost instantaneous and occurs practically exclusively by the added co-antioxidant; the resulting radicals do not absorb at the wavelength we use for monitoring **ResO•**.

2 Properties of the species derived from resveratrol ResOH

2.1 Ground state and first excited singlet state

ResOH only absorbs in the UV. Figure S2 displays its longest-wavelength absorption band, which is in good agreement with literature data.[S7,S8] The spectrum does not change in the pH range

from 3 to 7, but shifts at higher pH owing to the deprotonation of the phenolic hydroxyl groups of **ResOH** (first pK_a, 9.3)[S9]. To ensure the absence of deprotonated substrate **ResO**$^-$, we, therefore, carried out the laser flash photolysis experiments at pH 6.5. We excited **ResOH** at 355 nm, that is, almost at its long-wavelength absorption edge. At 355 nm, all our co-antioxidants are fully transparent, but **ResOH** still absorbs strongly enough ($\varepsilon_{355} = 850\,\mathrm{M^{-1}\,cm^{-1}}$) for a sufficient degree of photoionization.

To determine the molar absorption coefficient of the *cis*-isomer, we irradiated a solution of **ResOH** with an HBO 50 mercury lamp through a 360 nm cutoff filter for 2 minutes, and then separated the spectra of the isomer mixture using the known ratio of molar absorption coefficients at 304 nm ($\varepsilon_{trans}/\varepsilon_{cis} = 3.19$)[S10]. This gave a value of 200 $\mathrm{M^{-1}cm^{-1}}$ at 355 nm.

In SDS micelles, the molar absorption coefficient of **ResOH** was found to be 1150 $\mathrm{M^{-1}cm^{-1}}$ at 355 nm. The value for the *cis*-isomer was not determined.

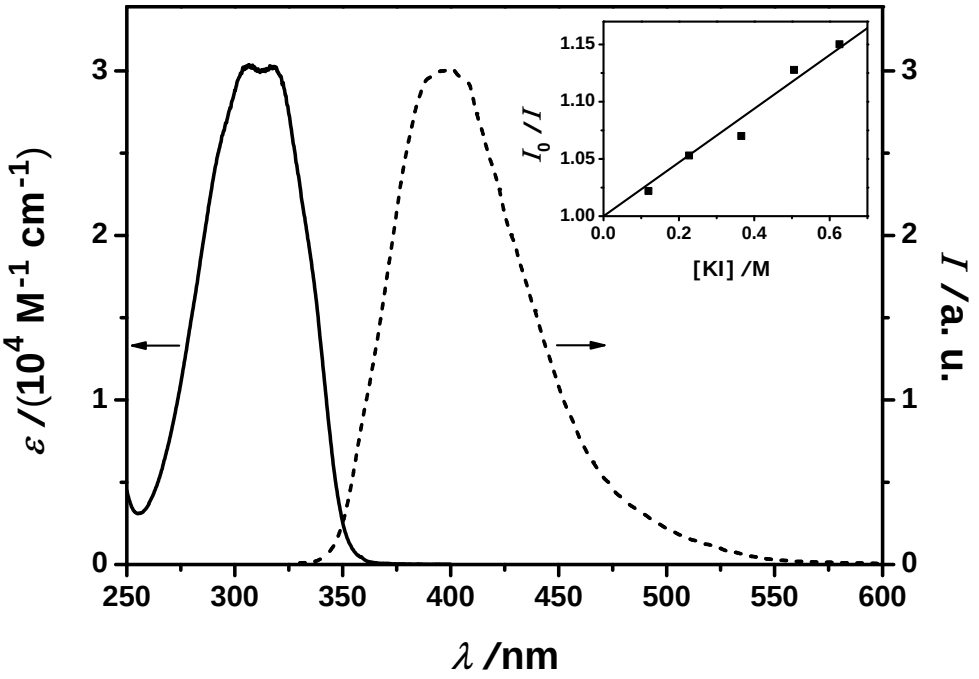

Figure S2: Main plot, calibrated absorption spectrum of **ResOH** (solid line) and normalized fluorescence spectrum of **ResOH** (dashed line). Inset, Stern-Volmer plot for the fluorescence quenching of **ResOH** (2×10^{-5} M) by potassium iodide at pH 6.5. Excitation wavelength for all fluorescence measurements, 305 nm. For further details, see text.

Phenols typically exhibit an increased acidity in the first excited singlet state by 5–6 pK units,[S11] which manifests itself by changes of the fluorescence spectrum when the pH is varied. However, we observed identical fluorescence spectra between pH 3 and pH 7, which indicates that in this pH range the first excited singlet state of resveratrol ***ResOH**(S_1) does not undergo an excited-state proton transfer to the solvent. Hence, the intermediate in the biphotonic (see, main paper) near-UV photoionization of **ResOH** is ***ResOH**(S_1); a contribution of the excited phenolate ***ResO**$^-$(S_1) can be ruled out.

To obtain the lifetime of ***ResOH**(S_1), we carried out a Stern–Volmer experiment with iodide,

which has already been used for lifetime determinations of numerous organic compounds[S12] and does not absorb at the excitation wavelength chosen by us (305 nm). The resulting Stern–Volmer plot is linear (Figure S2, inset) with a Stern–Volmer constant of 0.235 M^{-1}. Assuming diffusion-controlled quenching between species without a Coulombic interaction ($k_q = 6.5 \times 10^9\ M^{-1}\ s^{-1}$)[S12] the lifetime of ***ResOH**(S_1) is calculated to be 36 ps, a typical value for stilbene derivatives[S13].

2.2 Phenoxy radical ResO•

2.2.1 Quantum mechanical calculations

All computations were carried out with the Gaussian 09 package.[S14] We calculated the vertical excitation energies of **ResO•** with Time-Dependent Density Functional Theory (TD-DFT), which has already been used successfully for the prediction of absorption spectra of numerous organic dyes.[S15] Before that, we performed a geometry optimization and a frequency analysis of **ResO•**. We used an enlarged basis set (6-311++G(2d,2p)) for all computations of the open-shell species, the pure BLYP functional, which frequently reproduces absorption spectra better than hybrid functionals such as B3LYP or B3P86,[S16] and the solvation model IEFPCM with the solvent water. The orbitals were obtained by a single-point calculation with population analysis.

Figure S3 displays the optimized structure of **ResO•**. The calculated electronic transitions with their corresponding oscillator strengths are summarized in Table S1; for the two strongest transitions, these data have also been plotted in Figure 1a of the main paper.

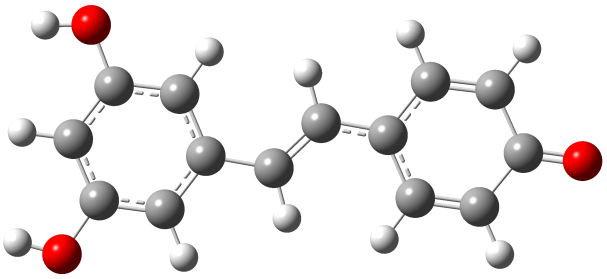

Figure S3: Optimized structure of **ResO•** at the BLYP/6-311++G(2d,2p) level of theory. For details, see text.

E / eV	λ / nm	oscillator strength
1.085	1142.3	0.0007
1.152	1076.0	0.0000
1.691	733.2	0.1516
2.218	559.1	0.0031
2.367	523.8	0.0477
2.901	427.4	0.8364
2.975	416.8	0.0458
3.201	378.4	0.0000
3.330	372.3	0.0000
3.337	371.5	0.0375
3.355	369.5	0.0629
3.589	345.5	0.0828

Table S1: Computed vertical excitation energies (E), corresponding wavelengths (λ) and oscillator strengths for the electronic transitions of **ResO•** in the IR, visible and near-UV.

Based on our calculations, the first allowed electronic transition (indicated by a notable oscillator strength) of **ResO•** lies at 733.2 nm and corresponds to the SOMO − 3 → SOMO

transition (these orbitals are shown in Figure S4). All theoretical results, in particular the two main transitions, which are highlighted in Table S1, are in excellent agreement with the experimentally observed spectrum (compare, Figure 1a of the main article).

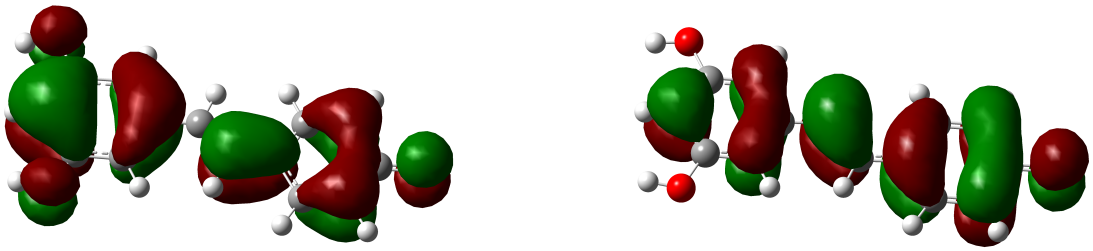

Figure S4: Computed orbitals of **ResO$^\bullet$** that are involved in the first allowed electronic transition. Left, orbital 57 (SOMO − 3); right, orbital 60 (SOMO). Further details, see text.

2.2.2 Spectral calibration

We calibrated the extinction coefficient of **ResO$^\bullet$**, $\varepsilon\left(\mathbf{ResO^\bullet}\right)$, by three independent approaches, which all gave the same result.

a) In the photoionization experiments on **ResOH** alone, determining $\varepsilon\left(\mathbf{ResO^\bullet}\right)$ from the slopes in the inset of Figure 1a of the main paper using the well-known $\varepsilon\left(\mathbf{e_{aq}^{\bullet-}}\right)$ as reference is a straightforward procedure.

That calibration is based simply on equating the post-flash concentrations of $\mathbf{e_{aq}^{\bullet-}}$ and **ResO$^\bullet$**, which follows from the stoichiometry of the electron detachment, Equation S2,

$$^*\mathbf{ResOH} \longrightarrow \mathbf{ResO^\bullet} + \mathbf{e_{aq}^{\bullet-}} + H^+ \qquad \text{(S2)}$$

A violation of that stoichiometry could only be caused by a parallel hydrogen ejection from *the same* excited state according to Equation S3 (the linearity of the plots in the insets of Figure 1a of the main paper rules out any additional route to **ResO$^\bullet$** via a different excited state).

$$^*\mathbf{ResOH} \longrightarrow \mathbf{ResO^\bullet} + H^\bullet \qquad \text{(S3)}$$

In the case of parallel Reactions S2 and S3, method a) would merely yield an upper limit to the true $\varepsilon\left(\mathbf{ResO^\bullet}\right)$. However, Reaction S3 was undetectable in 355 nm laser flash photolysis of **ResOH** in acetonitrile,[S17] so we consider it as equally unlikely in our medium, which is corroborated by the absence of an H/D kinetic isotope effect on the slopes in the inset of Figure 1a of the main paper.

b) The absorptions directly after the flash in the experiment of Figure 2a of the main paper, *i.e.*, with added co-antioxidant **HAsc$^-$** in N_2O-saturated solution, allow a calibration of $\varepsilon\left(\mathbf{ResO^\bullet}\right)$ against the previously determined[S1] $\varepsilon\left(\mathbf{Asc^{\bullet-}}\right)$.

The rationale behind this is that both $\mathbf{OH^\bullet}$ and $\mathbf{H^\bullet}$ rapidly react with $\mathbf{HAsc^-}$. At the concentration of $\mathbf{HAsc^-}$ in that experiment, 10 mM, the reaction with $\mathbf{OH^\bullet}$ to give $\mathbf{Asc^{\bullet-}}$ is too fast to be reliably resolved with our setup ($k = 1.1 \times 10^{10}\,\mathrm{M^{-1}s^{-1}}$)[S4], and $\mathbf{OH^\bullet}$ is itself the product of the quasi-instantaneous and quantitative scavenging of $\mathbf{e^{\bullet-}_{aq}}$ by N_2O according to Reaction S1; the reaction with $\mathbf{H^\bullet}$, affording an unspecified radical $\mathbf{X^\bullet}$, would have a time constant of 330 ns ($k = 3 \times 10^8\,\mathrm{M^{-1}s^{-1}}$)[S4], that is, would be easily observable with our system but much faster than the secondary rise of $\mathbf{Asc^{\bullet-}}$. We did not detect any such fast component in our kinetic spectra. That absence, unless $\mathbf{X^\bullet}$ were nonabsorbing throughout the whole spectral range investigated, further supports that Reaction S3 plays no role in our system. Method b) thus captures the radicals accompanying $\mathbf{ResO^\bullet}$ formation in the same way as method a), and additionally sustains that the reaction is uniform.

c) The slower absorption changes after the laser flash in the same experiment as in b) provide a third calibration, which again compares $\varepsilon\left(\mathbf{ResO^\bullet}\right)$ to $\varepsilon\left(\mathbf{Asc^{\bullet-}}\right)$:

The correlated decrease to zero of the $\mathbf{ResO^\bullet}$ absorbance and increase of the $\mathbf{Asc^{\bullet-}}$ absorbance, as opposed to the almost complete stability of $\mathbf{ResO^\bullet}$ in the absence of $\mathbf{HAsc^-}$ (see, Figure 2b of the main paper) and the constant concentration of $\mathbf{Asc^{\bullet-}}$ on that timescale in photoionization experiments on $\mathbf{HAsc^-}$ itself,[S1] rule out any independent source of $\mathbf{ResO^\bullet}$ decay and $\mathbf{Asc^{\bullet-}}$ formation other than that given by Reaction S4,

$$\mathbf{ResO^\bullet} + \mathbf{HAsc^-} \longrightarrow \mathbf{ResOH} + \mathbf{Asc^{\bullet-}} \tag{S4}$$

so provides a third stoichiometric relationship that can be used for calibrating $\varepsilon\left(\mathbf{ResO^\bullet}\right)$.

The high signal-to-noise ratio of our measurements (compare, the experimental traces in the main paper and the Supporting Information) makes these calibrations very precise. Based on the practically perfect agreement between the extinction coefficients obtained by methods a)–c), $\varepsilon_{410} = 33400\,\mathrm{M^{-1}\,cm^{-1}}$, we also expect it to be quite accurate, in particular because each calibration method derives all its observables from the same experiment on the same sample, thereby completely removing uncertainties of the excitation or the optical path length.

2.2.3 Stability in the absence of co-antioxidants

In N_2O-saturated solutions of $\mathbf{ResOH}$, the instantaneous rise of $\mathbf{ResO^\bullet}$ at the moment of the photoionizing laser pulse is followed by a slow secondary increase, which is caused by the reaction of surplus $\mathbf{ResOH}$ with hydroxyl radicals (the product of scavenging $\mathbf{e^{\bullet-}_{aq}}$ by N_2O, as discussed in Section 1). This kinetic behaviour can be seen very clearly in the black trace of Figure S5.

To study the $\mathbf{ResO^\bullet}$ stability, we avoided the formation of hydroxyl radicals by working in Ar-saturated solution, and extracted the contribution of $\mathbf{ResO^\bullet}$ to the 410 nm trace (Figure S5, green trace), which comprises only the absorptions of $\mathbf{e^{\bullet-}_{aq}}$ and $\mathbf{ResO^\bullet}$, in the following way:

We separately monitored $\mathbf{e}_{aq}^{\bullet-}$ by a difference experiment at 824 nm, multiplied that difference trace with the pertaining ratio of the molar absorption coefficients of $\mathbf{e}_{aq}^{\bullet-}$ ($\varepsilon_{824}/\varepsilon_{410} = 0.17$), and subtracted the result from the 410 nm trace recorded in Ar-saturated solution. The pure **ResO•** signal so obtained (Figure S5, dark red trace) decreases by 2 % at most during the experiment, clearly indicating the stability of **ResO•** in water on a timescale of at least tens of microseconds. The described procedure for extracting the **ResO•** signal leads to the same result at 650 nm. Because it is very unlikely that any absorbing decay products of $\mathbf{e}_{aq}^{\bullet-}$ would contribute identically at both detection wavelengths, these measurements are seen to be undisturbed by such products, so yield the pure time-dependence of the **ResO•** concentration.

ResO• is reported to undergo a further deprotonation at a pH of about 7.[S6] However, we recorded kinetic spectra of **ResO•** at pH 5.5 and pH 6.5 and did not observe any difference. Furthermore, the yields of **ResO•** and $\mathbf{e}_{aq}^{\bullet-}$ were equal under both conditions.

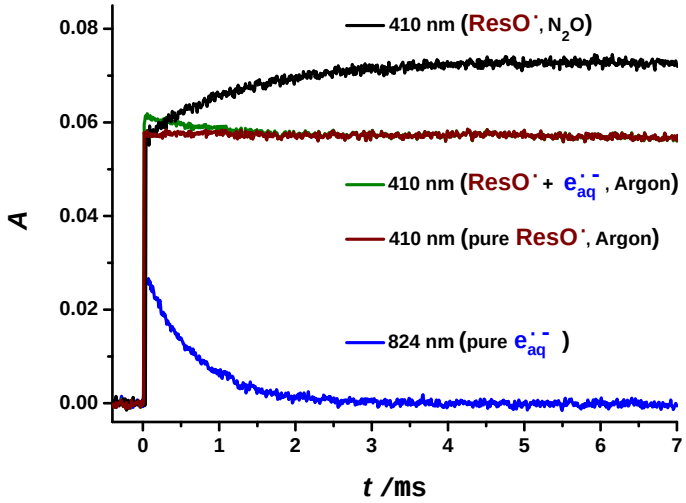

Figure S5: Experimental traces following the 355 nm laser flash photolysis (349 mJ cm^{-2}) on an aqueous solution of 8×10^{-5} M **ResOH** at pH 6.5. The pure **ResO•** signal at 410 nm (dark red) was extracted from the 410 nm absorption trace (Ar-saturated solution, green) and the pure $\mathbf{e}_{aq}^{\bullet-}$ absorption at 824 nm (blue, compare Figure S1) by weighing the latter trace with the factor 0.17 and subtracting the result from the former trace. The trace recorded at 410 nm in N_2O-saturated solution (black) illustrates the further absorption increase due to the reaction of **ResOH** with hydroxyl radicals. For details, see text.

3 Photoionization

The kinetic model has been described in detail in a previous publication.[S18] A steady-state approximation for the concentration of the first excited state S_1 of **ResOH** during the laser pulse becomes the more accurate the higher the ratio τ_L/τ_S is (τ_L, duration of the laser pulse; τ_S, lifetime of S_1); in our experiments, where that ratio amounts to as much as 140, the approximate

intensity dependence given by Equation S5 is numerically indistinguishable from the much more complicated exact result.

$$\left[\mathbf{e}_{\mathbf{aq}}^{\bullet-}\right]/c_0 \quad = \quad 1-\exp\left(-\frac{aI^2}{1+bI}\right) \tag{S5}$$

Equation S5 expresses the electron concentration relative to the substrate concentration c_0 as function of the excitation intensity I in terms of two parameters a and b, which are themselves composed of τ_L/τ_S and two photokinetic constants describing the primary excitation and the ionization proper, respectively. These relationships,[S18] which are not repeated here, can be rearranged to give Equation S6,

$$\varepsilon\left(S_0\right) \times \frac{a}{b^2} \times \frac{\tau_L}{\tau_S} \quad = \quad \varepsilon\left(S_1\right) \times \varphi_{ion} \tag{S6}$$

As a small complication, $\varepsilon\left(S_0\right)$ in Equation S6 is a mixed molar absorption coefficient because the stationarity for S_1 during the laser pulse implies a stationarity between the *trans* and *cis* isomers of **ResOH** in their S_0 states. Assuming equal probabilities for the deactivation of S_1 to each geometrical isomer, $\varepsilon\left(S_0\right)$ is given by Equation S7,

$$\varepsilon\left(S_0\right) \quad = \quad \varepsilon_{trans} \times \frac{2}{1+\varepsilon_{trans}/\varepsilon_{cis}} \tag{S7}$$

The experimentally accessible quantity on the left-hand side of Equation S6 equals the product of the molar absorption coefficient of S_1 with the quantum yield φ_{ion} of ionizing S_1 with the second photon. With the molar absorption coefficients of Section 2.1 and the best-fit parameters a and b of Figure 1 in the main paper, $a = 1.0 \times 10^{-6}\,\mathrm{cm^4/mJ^2}$, $b = 3.7 \times 10^{-3}\,\mathrm{cm^2/mJ}$, it is seen to be $3300\,\mathrm{M^{-1}cm^{-1}}$ in water. That number constitutes the smallest possible molar absorption coefficient of S_1 at 355 nm (otherwise φ_{ion} would have to exceed 1), and in turn allows an estimation of the minimum value of φ_{ion}: The S_1 absorption spectrum in acetonitrile appears to exhibit a minimum in that wavelength range, with a molar absorption coefficient of at most one sixth of the maximum at around 520 nm;[S17] assuming a theoretical maximum of $100000\,\mathrm{M^{-1}cm^{-1}}$ for the latter peak, φ_{ion} should, therefore, be at least 0.2.

The significantly larger electron yield in SDS (see, Figure 1b of the main paper; best-fit parameters, $a = 2.6 \times 10^{-6}\,\mathrm{cm^4/mJ^2}$, $b = 5.3 \times 10^{-3}\,\mathrm{cm^2/mJ}$) can be traced back predominantly to a higher $\varepsilon\left(S_0\right)$ owing to a small red shift of the ground-state spectra; the increase of the pertaining parameter b by a factor of 1.4 directly reflects the increase of the ground-state molar absorption coefficient.

4 Repair reaction of ResO$^\bullet$, and co-antioxidant-derived radicals

All co-antioxidants used to repair **ResO$^\bullet$** neither absorb at our laser wavelength (355 nm) nor quench ***ResOH**(S_1) at the applied concentrations and thus do not influence the **ResO$^\bullet$** generation by near-UV photoionization. These concentrations were, ascorbate, 2–10 mM; 4-aminophenol, 3–6 mM; trolox, 1–3 mM; cysteine, 70–400 mM; glutathione, 5–50 mM.

Furthermore, their radicals, which are produced either by the repair of **ResO$^\bullet$** or by the scavenging of hydroxyl radicals, do not absorb above 600 nm. The absorption maxima of these radicals lie at 360 nm for ascorbate ($\varepsilon = 4500\ M^{-1}cm^{-1}$)[S1], 440 nm for 4-aminophenol,[S5] 435 nm for trolox,[S19] and at 410 nm for the dimeric cysteine and glutathione radical anions,[S20] which are the only thiol-derived species absorbing in our detection range.

Supporting References

[S1] C. Kerzig and M. Goez, *Phys. Chem. Chem. Phys.*, 2014, **16**, 25342–25349.

[S2] P. M. Hare, E. A. Price and D. M. Bartels, *J. Phys. Chem. A*, 2008, **112**, 6800–6802.

[S3] J. W. T. Spinks and R. J. Woods, *An Introduction to Radiation Chemistry*, Wiley, New York, 2nd edn, 1976.

[S4] G. V. Buxton, C. L. Greenstock, W. P. Helman and A. B. Ross, *J. Phys. Chem. Ref. Data*, 1988, **17**, 513–886.

[S5] T. S. Singh, S. P. Gejji, B. S. Madhava Rao, H. Mohan and J. P. Mittal, *J. Chem. Soc., Perkin Trans. 2*, 2001, 1205–1211.

[S6] S. Stojanović and O. Brede, *Phys. Chem. Chem. Phys.*, 2002, **4**, 757–764.

[S7] T. S. Figueiras and M. T. Neves-Petersen, *J. Fluoresc.*, 2011, **5**, 1897–1906.

[S8] M. A. Vian, V. Tomao, S. Gallet, P. O. Coulomb and J. M. Lacombe, *J. Chromatogr. A*, 2005, **1085**, 224–229.

[S9] M. Deak and H. Falk, *Monatsh. Chem.*, 2003, **134**, 883–888.

[S10] L. Camont, C.-H. Cottart, Y. Rhayem, V. Nivet-Antoine, R. Djelidi, F. Collin, J.-L. Beaudeux and D. Bonnefont-Rousselot, *Anal. Chim. Acta*, 2009, **634**, 121–128.

[S11] J. R. Lakowicz, *Principles of Fluorescence Spectroscopy*, Springer, New York, 3rd edn, 2006.

[S12] M. Montalti, A. Credi, L. Prodi and M. T. Gandolfi, *Handbook of Photochemistry*, Taylor and Francis, Boca Raton, 3rd edn, 2006.

[S13] S. Samori, M. Hara, S. Tojo, M. Fujitsuka and T. Majima, *J. Photochem. Photobiol. A: Chem.*, 2006, **179**, 115–124.

[S14] M. J. Frisch, G. W. Trucks, H. B. Schlegel, G. E. Scuseria, M. A. Robb, J. R. Cheeseman, G. Scalmani, V. Barone, B. Mennucci, G. A. Petersson, H. Nakatsuji, M. Caricato, X. Li, H. P. Hratchian, A. F. Izmaylov, J. Bloino, G. Zheng, J. L. Sonnenberg, M. Hada, M. Ehara, K. Toyota, R. Fukuda, J. Hasegawa, M. Ishida, T. Nakajima, Y. Honda, O. Kitao, H. Nakai, T. Vreven, J. A. Montgomery, Jr., J. E. Peralta, F. Ogliaro, M. Bearpark, J. J. Heyd, E. Brothers, K. N. Kudin, V. N. Staroverov, R. Kobayashi, J. Normand, K. Raghavachari, A. Rendell, J. C. Burant, S. S. Iyengar, J. Tomasi, M. Cossi, N. Rega, J. M. Millam, M. Klene, J. E. Knox, J. B. Cross, V. Bakken, C. Adamo, J. Jaramillo, R. Gomperts, R. E. Stratmann, O. Yazyev, A. J. Austin, R. Cammi, C. Pomelli, J. W. Ochterski, R. L. Martin, K. Morokuma, V. G. Zakrzewski, G. A. Voth, P. Salvador, J. J. Dannenberg, S. Dapprich, A. D. Daniels, Ö. Farkas, J. B. Foresman, J. V. Ortiz, J. Cioslowski and D. J. Fox, *Gaussian 09 Revision A.1*, Gaussian Inc., Wallingford CT, 2009.

[S15] D. Jacquemin, E. A. Perpète, G. E. Scuseria, I. Ciofini and C. Adamo, *J. Chem. Theory Comput.*, 2008, **4**, 123–135.

[S16] W. Li, Y.-B. Wang, I. Pavel, Q. Yuan, Y. Ye, E.-Q. Fu, M.-D. Luo, J.-M. Hu and W. Kiefer, *J. Phys. Chem. A*, 2005, **109**, 2878–2886.

[S17] I. Džeba, T. Pedzinski and B. Mihaljević, *J. Photochem. Photobiol. A*, 2015, **299**, 118–124.

[S18] M. Goez and C. Kerzig, *Angew. Chem. Int. Ed.*, 2012, **51**, 12606–12608.

[S19] M. J. Davies, L. G. Forni and R. L. Willson, *Biochem. J.*, 1988, **255**, 513–522.

[S20] M. Z. Hoffman and E. Hayon, *J. Phys. Chem.*, 1973, **77**, 990–996.